Amplification of UV radiation and gain mechanisms in ZnO films with loose-packed structure

L.A. Zadorozhnaya [1], A.P. Tarasov [1], A.S. Lavrikov [1], V.M. Kanevsky [1]
[1] Shubnikov Institute of Crystallography,
Federal Scientific Research Centre "Crystallography and Photonics", NRC "Kurchatov Institute",
119333, Moscow, Russia, Leninskiy pr. 59

Abstract

The modern demands for miniaturization of optoelectronic devices, in particular, for the UV range, are inextricably linked with the improvement of fabrication technologies for the corresponding photonic nano/micro objects and the study of their radiative properties. In this work, the method of pyrolytic carbothermal synthesis, which is a modification of the thermal evaporation method, was used to fabricate microcrystalline ZnO films with laser properties. The influence of the size and packing type of ZnO microcrystallites in the films on their emissive properties were revealed. The films with relatively large microcrystallites (10 – 15 μm in size on average) were found to exhibit UV amplified spontaneous emission at room temperature. The possibility of additional enhancement of this emission and its two-threshold behavior in loose-packed regions of such films were found for the first time. It was shown that the observed phenomenon is due to the competition between two gain mechanisms, which are assumed to arise predominantly in different regions of microcrystallites as a result of exciton-phonon and exciton-electron interaction processes. As the temperature decreases, the dominant gain mechanism gradually changes to exciton-exciton scattering, regardless of the type of film structure. The results obtained open up the possibilities of the thermal evaporation synthesis to a wider extent and can be useful in interpreting the optical gain mechanisms in ZnO micro- and nanostructures.

Keywords: ZnO film, loose-packed structure, UV laser, amplified spontaneous emission, emission enhancement, exciton gain.

Citation: Zadorozhnaya LA, Tarasov AP, Lavrikov AS, Kanevsky VM. Amplification of UV radiation and gain mechanisms in ZnO films with loose-packed structure. Computer Optics 2024; 48(5): 696-704. DOI: 10.18287/2412-6179-CO-1414.

Acknowledgements: The study was supported by the grant of the Russian Science Foundation (grant *N*o. 23-29-00535, https://rscf.ru/en/project/23-29-00535/).

Introduction

Zinc oxide is a well-known and important material for the semiconductor industry, in particular electronics and optoelectronics. Due to its direct wide band gap (3.37 eV at room temperature), high exciton binding energy (60 meV), high electron mobility, as well as non-toxicity and radiation resistance, ZnO can be used for a wide range of optoelectronic and photonic devices for the UV and blue ranges [1 – 3]. Ample opportunities exist for growing ZnO micro- and nanostructures with a wide range of morphologies [2 – 6]. Some of them provide light confinement and amplification [7 – 9], which is an essential factor for miniaturization of photonic devices. Due to a high quantum yield and gain for near-band-edge (NBE) emission, ZnO allows effective excitation of room temperature (RT) UV luminescence and lasing [10], which makes it useful in the development of both UV LEDs and laser sources.

Among the methods of high-temperature synthesis of ZnO structures, perhaps the simplest is the method of thermal evaporation [3, 10]. High synthesis temperatures (usually more than 900–1000°C) allows achieving high crystalline and optical quality of growing structure, which in many cases provides them with good luminescent characteristics [11, 12]. The method does not use a carrier gas and allows the synthesis to be carried out in an air atmosphere, which makes it relatively simple. However, on the other hand, this leaves fewer opportunities for controlling the synthesis process. As a result, fast uncontrolled growth of crystallites in most cases leads to the formation of mainly filamentous nano- and microstructures in the form of rods, wires, etc. It is difficult to use this method for obtaining ZnO crystals of a different shape and larger micron size, including microfilms and microcrystals with the properties of a bulk material.

As an alternative to the thermal evaporation method, in the 2000s the method of pyrolytic carbothermal synthesis (PCS) was proposed and subsequently improved [13, 14]. The PCS method does not use a carrier gas and utilizes oxygen directly from air to synthesize the oxide, thereby retaining the advantages of the thermal evaporation method. On the other hand, the high functionality of PCS was shown, comparable with more complex methods, in particular, the vapor transport synthesis. PCS is able to provide growth both by vapor-solid (VS) and vapor-liquid-solid (VLS) mechanisms. The implementation of the VS model of growth allows obtaining oxide powders [13, 14] in a sufficiently large amounts in a one experiment, which scales up the method. In its turn, VLS

growth makes it possible to fabricate oxide structures on substrates, e.g., aligned ZnO microrods [15]. For the growth of ZnO structures, any Zn-containing compounds, both of organic and inorganic nature, that allow oxide formation during pyrolysis at temperatures up to 900°C can theoretically be used as a source material. In this case, the following growth scheme is realized: decomposition of a Zn-containing compound → formation of ZnO → reduction of ZnO to metallic Zn → sublimation of Zn vapors → oxidation of Zn vapors with atmospheric oxygen → formation of ZnO crystallites. If ZnO or Zn powders are used as a source material for the growth of ZnO structures, the first or both first and second stages, respectively, in the aforementioned scheme can be omitted.

The high efficiency of the PCS method for fabricating ZnO laser micro- and nanostructures was shown. ZnO structures exhibiting both Fabry-Perot mode (FPM) lasing [13, 16] and whispering gallery mode (WGM) lasing [15, 16] were synthesized. In particular, low-threshold WGM lasing in ZnO crystallites with a hexagonal cross section of both small, submicron diameter [16] and large, up to 20 μm, diameter [15] was obtained and *Q*-factors sufficiently high for as-grown microcrystals (up to 3000 – 3500) were reached [15].

In this work, we demonstrate the possibility to use the PCS method for creating luminescent ZnO film structures. This brings the capabilities of this method even closer to the functionality of the vapor transport synthesis [17 – 19], but with much greater simplicity and safety. We have revealed the influence of the sizes of film microcrystallites and the photoexcitation intensity on the radiation behavior of the films and the possibility of excitation of amplified spontaneous emission (ASE) in the near UV range at RT. Some films with loose-packed structure of the microcrystallites exhibited a two-threshold character of ASE. The emission intensity in such cases was higher than for classical ASE with one interval of superlinear growth. The purpose of this work is to study the radiative properties and features of the fabricated ZnO films. In particular, the origin, behavior, and mechanisms of optical gain in such structures were of primary interest.

1. Materials and Methods

ZnO films were grown on *C*-plane sapphire substrates using the PCS method. Zinc granules with a purity of 99.999 % (Alfa Aesar, USA, MA) with a total weight of 250 mg were used as a precursor. The decalcified paper filter served as a porous cellulose carrier for a catalysis of the production of zinc vapor, which is an intermediate reaction product during further oxidation and ZnO growth. Thermal treatment at high temperature (1000 – 1100°C) was conducted; heating rate was 4.2 deg/min. The holding at constant temperature was 30 min. The synthesis was performed in high purity alundum crucibles in air ambient. The subsequent cooling down to RT was provided during ~ 20 h. The scheme of the experiment and the theory of the PCS method are given in more detail elsewhere [14]. This paper presents the results for two films synthesized in one experiment but with different amounts of air (the source of oxygen), which was ensured by different distances (15 mm and 40 mm) from the films to the window in the crucible. Different morphology of the films obtained in this way allows finding out the influence of the size of the microcrystallites and their packing density on the emission properties of the films. The film that was closer to the air source (window) and characterized by a large microcrystallite size is designated as film A in this work. The second film, located further from the air source and having relatively small microcrystallites, is designated as film B.

Microscopic studies of the samples were carried out via scanning electron microscopy (SEM), using a Jeol JSM-6000PLUS microscope.

Excitation of the samples' photoluminescence (PL) was performed with a frequency-tripled pulsed Nd:YAG laser (the wavelength, pulse duration and repetition rate are 355 nm, 10 ns and 15 Hz, respectively). The laser beam made an angle of ~ 40° with the sample's surface. The size of the excitation spot on the sample was ~ 120 μm. The emission of the sample was collected in the direction close to the normal to its surface and collimated to the entrance slit of a monochromator coupled to a charge-coupled device (CCD) camera. A signal accumulation of 50 – 100 laser pulses was used to enhance the signal-to-noise ratio. The emission spectra were corrected taking into account the sensitivity of the CCD array. Low temperature experiments were carried out using an optical nitrogen cryostat. The temperature of the samples was controlled using a Fe-CuNi thermocouple.

2. Results

Fig. 1 shows micrographs of the synthesized ZnO films. Both films have a microcrystalline structure formed mainly by a single layer of microcrystallites, the size of which determines the thickness of the films.

Film A (Fig. 1*a*) has rather large microcrystallites with an average size of 10 – 15 μm (see also the inset in Fig. 1*a*), some microcrystallites reach 30 – 35 μm in size. In some areas, closer to the edges of film A, its structure exhibits loose packing; there are micron gaps between individual microcrystallites in such areas (one of such a region is indicated in Fig. 1*a*). The microcrystallites of film B (Fig. 1*b*), on the contrary, are relatively small with an average size of ~ 3 – 4 μm and constitute a close-packed structure. In many cases, a distinct hexagonal form of individual microcrystallites of both films is observed, which indicates their wurtzite crystal structure.

The RT spontaneous emission of both films, which was recorded in the near UV and visible ranges under *cw* low-intensity excitation and pulsed excitation with a relatively low power density ρ_{exc} ~ 20 kW/cm^2, had no significant differences. Fig. 2 shows typical spontaneous emission spectra of the films.

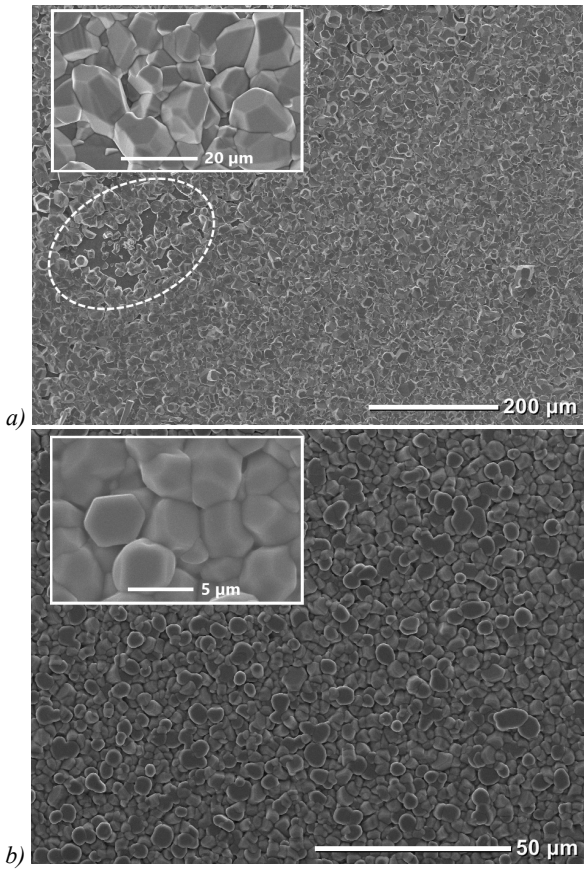

Fig. 1. Micrographs of the fabricated microcrystalline ZnO films: (a) film A (one of the film regions with loose packing is circled), (b) film B. The insets show enlarged images of microcrystallites

Upon low-intensity *cw* photoexcitation (Fig. 2*a*), the films emit only in the visible wavelength range. The maximum of this emission, known from the literature as deep-level (DL) emission, is in the green region at 515 nm (~2.4 eV) in the case under study. A different picture is observed for a pulsed excitation (Fig. 2*b*). In this case, in addition to DL emission, a relatively narrow band in the near UV region (maximum at ~380 nm) is also observed – this is NBE emission of ZnO. At this rather low intensity of pulsed excitation, this emission has a spontaneous nature as well. Such a cardinal change in the emission profile upon a significant increase of excitation power can be explained by the effects of saturation of DL emission centers at the high-density excitation and a decrease in the thickness of the depletion layer as a result of energy band flattening. In the second case, electron–hole pairs, intensively created by photons with an energy greater than the band gap, neutralize the excess charge on the semiconductor surface – the existence of this charge, in the absence of illumination, causes bending of the energy bands and formation of the depletion layer [20]. The straightening of the bands is accompanied by a partial deactivation of DL emission centers located near the surface and an increase in the probability of interband transitions. All this results in a relative increase in the UV component as compared to the visible one. However, the presence of DL emission even upon intense photoexcitation indicates that it fails to completely block the corresponding transitions.

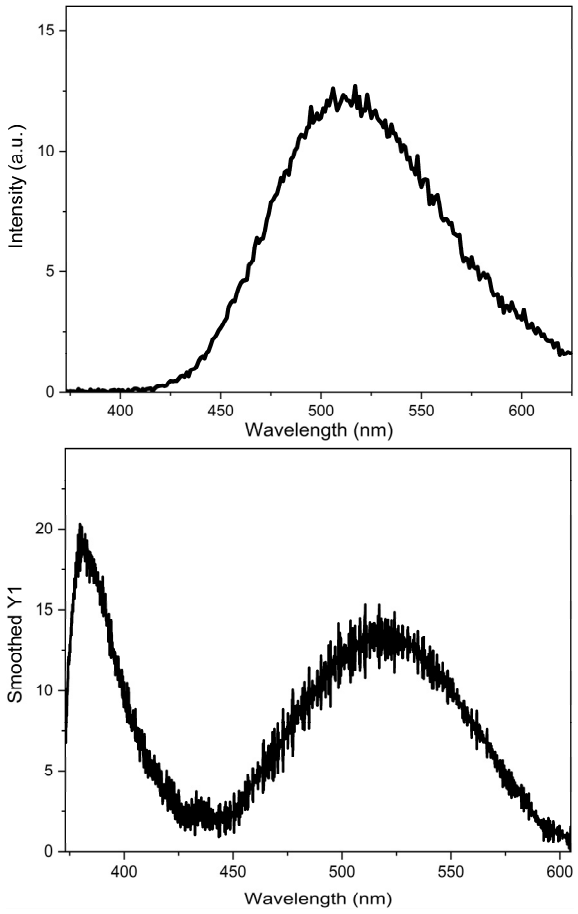

Fig. 2. Typical RT PL spectra of the films at cw excitation (a) and pulsed laser excitation with relatively low excitation power density, ρ_{exc} ~ 20 kW/cm^2 (b)

At higher intensities of pulsed excitation, the behavior of the films' NBE emission differs significantly. While film B demonstrates only spontaneous luminescence, film A exhibits amplified spontaneous emission (ASE) over almost entire film's area. Moreover, the highest intensity and the lowest threshold of ASE in film A were observed in the film regions corresponding to loose-packed structure. Fig. 3*a* shows the evolution of the PL spectra with increasing ρ_{exc} in one of such regions. For comparison, Fig. 3*b* shows the evolution of the spontaneous luminescence spectra of film B. Figs. 3*a* and 3*b* show fundamental differences between the two types of PL spectra. In the case of the film A, an increase in the excitation intensity leads to a transformation of the NBE emission spectrum. At ρ_{exc} less than ~25 kW/cm^2, a single spontaneous emission band at 381 nm is observed. As ρ_{exc} increases above 25 – 30 kW/cm^2, the second band emerges in the long-wavelength region of the first band (~390 nm). With a further increase in ρ_{exc}, the second band grows faster than the short-wavelength component and eventually makes up the main part of the spectrum. A comparison of the corresponding dependences of the full width at half maximum (FWHM) of the NBE emission spectra on ρ_{exc} in

two cases is shown in Fig. 3*c*. While the spontaneous luminescence band exhibits a gradual broadening with an increase in the excitation intensity, FWHM in the case of ASE first increases due to the appearance of a long-wavelength band, and then decreases, when it begins to dominate in the emission spectrum. At relatively high ρ_{exc}, the band becomes narrower than the initial spontaneous emission.

Fig. 3*d* compares the dependences of the integral intensity I_{int} of NBE emission on ρ_{exc} for both films. One can see that the behavior of the dependence $I_{int}(\rho_{exc})$ of film A differed clearly between the regions with loose and close packing types. In both cases, this dependence differs from linear or sublinear, which is usually observed in the case of spontaneous emission and is registered in the case of film B (Fig. 3*d*, squares). However, in contrast to the close-packed regions of film A, which show a superlinear growth typical to ASE (Fig. 3*d*, empty circles), in the loose-packed regions, the dependence $I_{int}(\rho_{exc})$ exhibits two intervals of superlinear growth (Fig. 3*d*, solid triangles circles). The first such interval (interval *II* in Fig. 3*d*) is located in the ρ_{exc} range ~ 25 – 50 kW/cm^2; it follows the linear interval of spontaneous luminescence (interval *I*) and ends with a tendency to saturation. The second superlinear segment (interval *III*) is observed at higher excitation intensities ($\rho_{exc} > 80$ kW/cm^2). These intervals (*I*, *II*, *III*) are also marked in Fig. 3*c*. The shape of the NBE emission spectrum and a behavior of its evolution with increasing ρ_{exc} do not differ significantly between different regions of the film A regardless of the packing type. However, in the case of loose-packed regions, a little faster redshift of the ASE band was observed in the initial interval of ρ_{exc} compared to the regions with close-packed crystallites. This is reflected in a generally longer wavelength position of ASE band (by 1.5 nm) in the PL spectra of loose-packed regions. At $\rho_{exc} > 160$ kW/cm^2, a small blue shift (by 0.3 nm) is also observed in this case.

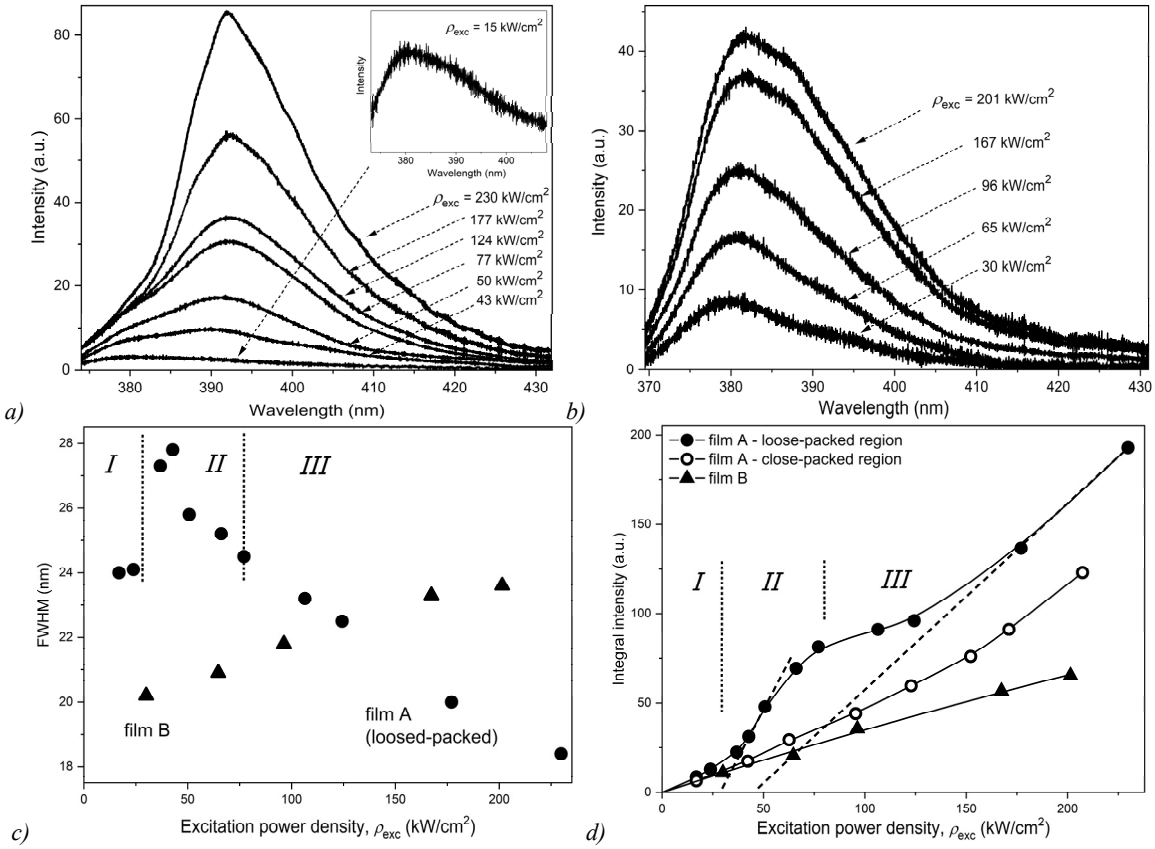

Fig. 3. (a, b) Room-temperature NBE emission spectra of the film A (loosed-packed region) (a) and the film B (b) at different excitation power densities ρ_{exc}, (c) FWHM vs. ρ_{exc} for the film A (loose-packed region) (circles) and film B (triangles), (d) the integral intensity of NBE emission I_{int} vs. ρ_{exc} for the loose-packed (solid circles) and close-packed (open circles) areas of the film A and for the film B (triangles); experimental points are connected by the solid lines for visual convenience. The designations I, II, and III in (c,d) indicate the feature intervals of the I_{int} (ρ_{exc}) dependence for the loose-packed area of the film A. The dashed lines in (d) show the maximum slope of the two superlinear segments (intervals II and III)

In order to establish the origin of the processes responsible for the optical gain in the film A structure, the temperature-dependent measurements of NBE emission of the films were performed. Fig. 4*a* shows the evolution of the NBE emission spectra of the film A at $T \sim 80$ K. Of note, the low-temperature spectra in all regions of the film were identical. At the lowest photoexcitation intensity (see the inset in Fig. 4*a*), the NBE emission pattern of the film is typical for nominally undoped micro/nano ZnO crystals with a high optical quality at this tempera-

ture [15,21 – 23] and coincides with that of the film B. In particular, four emission bands are clearly distinguishable (indicated as A_i, where $i = 1…4$ in Fig. 4*a*) with wavelengths of 370.1, 374.8, 383.6, and 392.7 nm (3.350, 3.308, 3.233, and 3.157 eV). These bands are due, respectively, to the recombination of bound excitons (A_1), the first phonon replica of free exciton radiation (*X*-LO) with a possible contribution of emission involving surface states (A_2), and the second (*X*-2LO) and third (*X*-3LO) phonon replicas of free exciton radiation (bands A_3 and A_4). Taking into account low surface-to-volume ratio of films' microcrystallites, the contribution of phonon replicas of emission bands related to surface defects in the energy range above ~ 3.25 eV is probably small [24].

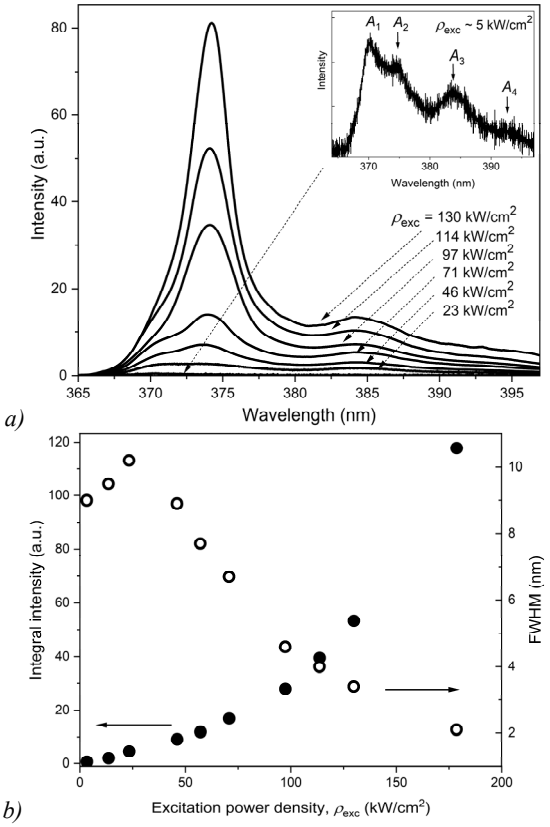

Fig. 4. (a) NBE emission spectra of the film A at different ρ_{exc} recorded at T = 80 K, (b) the corresponding dependences of the FWHM (open symbols) and the integral intensity (solid symbols) on ρ_{exc}

As the energy in the excitation pulse increases, beginning from approximately 10 – 20 kW/cm^2, the shape of the spectrum changes: the radiation intensity in the region of the A_2 band increases much faster than other parts of the spectrum. The dependences of I_{int} and FWHM measured in the spectral region of the $A_1 + A_2$ bands on ρ_{exc} are shown in Fig. 4*b*. One can see that the $I_{int}(\rho_{exc})$ dependence is superlinear over the entire excitation interval. FWHM, in general, demonstrates similar behavior to the RT case – in particular, a slight increase at the initial stage is associated with the appearance of the ASE band. This band exhibits a small redshift (~ 1 nm) in the ρ_{exc} range from ~ 50 to 180 kW/cm^2.

An emission band with such properties (characteristic wavelength, superlinear growth, weak redshift, low thresholds) is usually attributed to the recombination emission of excitons due to their scattering on each other (*X*-*X* scattering) and is called the *P*-band [22]. In our case, the correctness of attribution of the ASE band to *X*-*X* scattering can be verified by measuring the spectral distance from this band to, e.g., the *X*-2LO band (A_3). The energy of the *P*-band photon is given by the expression

$$P_n(T) = E_X(T) - E_b\left(1 - \frac{1}{n^2}\right) - \frac{3}{2}kT, \qquad (1)$$

where n is the number of the energy state to which one of the excitons transits ($n = 2, 3, ...$), $E_X(T)$ is the recombination energy of a free exciton, E_b is the exciton binding energy (60 meV in ZnO), 3/2 kT is the kinetic addition due to exciton movement.

The energy of photons emitted as a result of *X*-LO and *X*-2LO processes can be determined from the expression:

$$E_{X-mLO}(T) = E_X(T) - mE_{LO} + \left(\frac{5}{2} - m\right)k_BT, \qquad (2)$$

where $m = 1, 2$, E_{LO} is the energy of the LO phonon (72 meV in ZnO) [22]. Thus, the distance between the *P*-band and *X*-2LO emission should be 70 – 85 meV at 80 K for $n = 2, \ldots, \infty$. In our case, the minimum and maximum distances are 79 and 85 meV, respectively, which corresponds to theoretical values and allows us to attribute the observed ASE band to the *P*-band.

Fig. 5 shows the energy of the ASE band as a function of temperature for both types of microcrystallite packing in the film A at $\rho_{exc} \approx 60$ kW/cm^2, which corresponds approximately to the middle of the interval *II*. Also, the energies of the A_1, A_2 and A_3 spontaneous emission bands of the film B at $\rho_{exc} \approx 10$ kW/cm^2 are shown in Fig. 5.

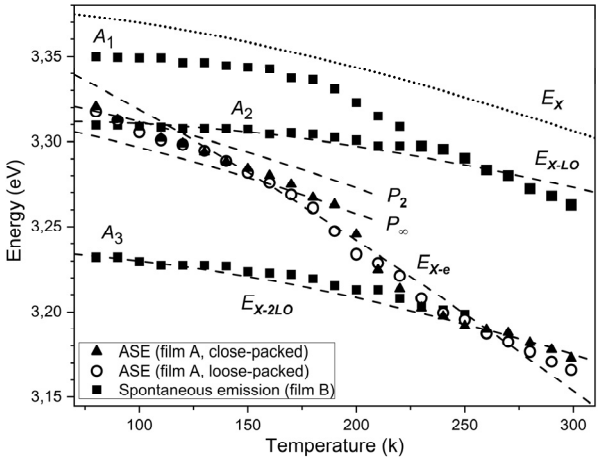

Fig. 5. Emission energy vs. temperature for ASE in the film A in the case of loose-packed (open circles) and close-packed (triangles) structures and spontaneous emission bands A_1, A_2 and A_3 of the film B (squares). Dashed lines indicate theoretical energies for $P_2(T)$, $P_\infty(T)$, $E_{X\text{-}LO}(T)$, $E_{X\text{-}2LO}(T)$, and $E_{X\text{-}el}(T)$ with $\gamma = 6$ calculated using $E_X(T)$ from [21] (indicated with a dotted line)

In order to clarify what mechanisms are involved in RT emission using the emission energy analysis, it is necessary to know the exciton energy $E_X(T)$ and/or band gap energy $E_g(T)$ of the samples. In this work, we are dealing with a structure consisting of fairly large microcrystallites fabricated under normal conditions without the use of additional doping. In addition, the structure of the NBE luminescence spectra of the films at low temperatures and low excitation intensities, as well as the energies of emission bands, are typical of bulk and microcrystalline ZnO. In this case, the data for bulk or microcrystalline ZnO can be used to interpret the gain mechanisms of the studied ZnO structure at various temperatures, including RT [15]. The dotted line in Fig. 5 shows the exciton transition energy $E_X(T)$ obtained for a bulk ZnO crystal in [21]; based on it, the dashed lines show the energies of the free-exciton processes aforementioned: *P*-band (1) at $n=2$ and $n=\infty$ and phonon replicas (2) at $m=1,2$.

Based on the obtained temperature dependences, some analysis of the emission bands origin can be performed. First, it can be seen that in the temperature range 80 – 160 K, the A_1 band approaches $E_X(T)$ from 23 meV to 13 meV. At $T>160$ K, the band rapidly moves away from $E_X(T)$. In the range of 80 – 160 K, the A_1 band is obviously due to the recombination of BXs, which gradually thermally dissociate as the temperature rises. Above $T\sim160$ K (the corresponding thermal energy is ~14 meV), when most of the BXs dissociated, the A_1 band is mainly due to zero-phonon exciton recombination; its energy approaches the A_2 band spectral region due to overlapping. The A_2 band quite strictly follows the energy $E_{X-1LO}(T)$, which proves the main contribution to it of the first phonon replica *X*-LO. At $T\sim230$ K, the A_1 and A_2 bands merge into one band, whose energy is slightly lower than the theoretical energy $E_{X-1LO}(T)$ at temperatures close to RT. The temperature behavior of A_3 band also confirms an attribution of it to the *X*–2LO emission. This band is clearly observed up to $T\sim250$ K. At $T>250$ K, it merges into the combined A_1+A_2 band, which possibly causes the redshift of its maximum away from theoretical dependence $E_{X-1LO}(T)$. Thus, the spontaneous emission of the fabricated microcrystalline films at RT is predominantly due to phonon replicas of free exciton emission (mainly *X*–LO), which corresponds to the case of bulk ZnO [25].

As the temperature rises, both ASE bands begin to shift from the P_2 energy at $T=80$ K, which is due to gradual increase of *n* in the X-X process. The band energy is within the *P*-band "corridor" between $n=2$ and $n=\infty$ up to 160 – 180 K. Then, a sharper redshift of the ASE band occurs. Zimmler et al. [26] associated a similar redshift of stimulated emission in ZnO nanowires with the temperature behavior of the absorption edge in ZnO. In particular, this effect can be caused by the process of emission reabsorption, increasing with temperature due to the developing Urbach tail. However, the interpretation of the redshift in large ZnO microcrystallites based on this phenomenon alone does not agree well with the observation of two different competing types of optical gain at RT and lower temperatures in such structures [15]. In this case, the effect of partial exciton ionization with increasing temperature seems to be more dominant [22, 27]. This process leads to the formation of another type of radiation as a result of the scattering of a free exciton by a free electron (*X*-el scattering). The photon energy $E_{X-el}(T)$ emitted due to this process is given by:

$$E_{X-el}(T)=E_x(T)-\gamma kT, \tag{3}$$

where γ is a coefficient that depends on the ratio of the effective masses of the exciton and the electron [22, 27]. In particular, in the interval between $T\sim160$ K and 260 K, the energy of the ASE band in the case of loose-packed structure is well described by the expression (3) with $\gamma=6$. This result corresponds to the experimental data for microcrystalline ZnO [15, 28] and satisfies the theory [22, 27]. The ASE band in the case of a close-packed structure experiences a sharper redshift and, after $T\sim240$ K, enters the theoretical curve $E_{X-2LO}(T)$ that describes the temperature behavior of the *X*-2LO process up to RT. In the case of a loose-packed structure, the ASE band remains between E_{X-2LO} and E_{X-el} with $\gamma=6$, as the temperature approaches RT.

3. Discussion

The data on temperature measurements and corresponding analysis allow us to perceive that at RT the contribution of *X*-e emission is significant in the sample's regions with loose packing in contrast to the region with close-packed microcrystallites, where optical gain is provided mainly by the *X*-2LO process. Given this, one can explain not only the fast local growth of the $I_{\text{int}}(\rho_{\text{exc}})$ in the interval *II* of excitation intensities used but also the RT behavior of the ASE band energy as a function of excitation intensity, in particular, the initial redshift of the band towards the theoretical *X*-e emission energy. This redshift saturates completely at the beginning of the second segment of the superlinear growth (interval *III*), and then (at $\rho_{\text{exc}}>150$ kW/cm^2) is replaced by the blueshift. This behavior may indicate changes in the gain mechanism involved in ASE at excitation intensities in the vicinity of the boundary of *II* and *III* intervals.

For example, taking into account that the first section of superlinear growth is associated with an exciton process, one could assume a change in the gain type from exciton to photon when population inversion occurs in the electron–hole plasma (EHP) – similar to polariton lasers, whose intensity vs. pumping dependence often exhibits similar behavior [29, 30]. The blue shift in this case could be explained by the dynamic Burstein–Moss effect (the band filling due to intensive creation of electron-hole pairs via photoexcitation) [31, 32]. However, in our case, taking into account the relatively low excitation intensities (the corresponding number of electron–hole pairs at the onset of ASE is no more than $\sim5\cdot10^{17}$ cm^{-3}) and ra-

ther long wavelength position of the ASE band, the achievement of population inversion in the EHP is unlikely [8, 30, 33]. Moreover, in microcrystalline structures, including fairly massive ZnO microcrystals, gain is most often achieved due to scattering of electron–hole pairs (excitons) rather than direct recombination in an inverted EHP [15, 22, 28, 33]. When the Mott threshold is exceeded, apparently, the transformation into mechanisms similar to excitonic ones takes place in the non-inverted EHP, since neither the spectral behavior of ASE with increasing excitation intensity, nor its temperature dependence exhibit significant changes. For example, Klingshirn et al. [33] proposed mechanisms that involve Coulomb-correlated electron-holes pairs in EHP as analogues to the *X*-e and *X*-*m*LO processes. In this case, the transition from the exciton regime to the EHP regime should occur smoothly, without sharp features in the $I_{int}(\rho_{exc})$ dependence.

Thus, the results obtained can be interesting not only as an expansion of the thermal evaporation method in the sense of creating lasing ZnO microfilm structures, but also as useful material for analyzing the gain mechanisms in ZnO micro- and nanoobjects. Despite extensive researches, the issue of the origin of UV stimulated emission in different ZnO structures, especially at RT, is still often controversial due to, among other things, a sufficiently large number of processes in ZnO that could potentially give rise to optical gain [10]. In particular, the stimulated emission band, excited in the region of ~ 389 – 392 nm (3.16 – 3.19 eV) and not showing an intense red-shift with an increase in the excitation intensity (i.e., similar to the closed-packed regions of the film A), is often observed in ZnO microstructures at RT, but its origin is debatable. In the present work, following our recent results [15], the connection of this emission to *X*-2LO process is confirmed. In addition, it is shown that this process can coexist at RT with *X*-e scattering, which is also capable of providing gain. Note that in geometrically high-quality ZnO microrods, RT gain is provided by *X*-e scattering alone – the gain due to X-2LO process is observed in such crystals only at lower temperatures, where it can also compete with the *X*-e gain [15].

A reason for the appearance of an inflection in the $I_{int}(\rho_{exc})$ dependence in the case of the loose-packed microcrystallites of the film A could be the saturation of the *X*-e emission with a rising excitation intensity. At the same time, *X*-2LO emission gradually increases and eventually becomes dominant. This is reflected in the appearance of superlinearity, which seems to be the second threshold of ASE, as well as in the saturation of the red-shift and the subsequent blueshift of the emission band at relatively high excitation intensities. The saturation of *X*-e radiation is indirectly confirmed by the similar character of $I_{int}(\rho_{exc})$ dependence in the interval *III* for both types of microcrystallites packing.

Such a behavior of the optical gain, namely *X*-e and *X*-2LO processes, can be explained by the peculiarities of the optical mode structure of microcrystallites of the film A, which clearly manifests itself in the film's regions with loose packing. The packing type, i.e., the presence or absence of pores, in two types of film regions is their only difference; the size and shape of the microcrystallites are identical in all parts of the film. As noted in the Introduction, both WGMs and FPMs can be formed in ZnO microcrystals grown by the PCS method. In the case of the films under study, the following scenario is probable. In the initial range of excitation intensities, near-surface WGM-like optical modes are excited. The interrelation of the gain provided by WGMs and, in particular, WGM lasing with the *X*-e process in large ZnO microcrystallites was demonstrated in [15]. At the same time, the geometric and structural perfection of crystals is an essential factor for observing lasing and, in general, stimulated emission of this type [9], including the cases when the *X*-e process is involved [15]. The microcrystallites of the film studied in this work often have a pronounced hexagonal shape, but in most cases, it is far from ideal hexagonal geometry with a clear hexagon in cross section and strict angles. As a result, on the one hand, the weak localization of WGM-type optical modes in film microcrystallites makes it impossible to overcome losses and begin lasing with a pronounced mode pattern. On the other hand, in the absence of sufficient gain, the radiative potential of the near-surface part of microcrystallites, which is filled with deep-level defects, is quickly exhausted with an increase in the excitation intensity. This results in saturation of the growth of the resonant emission. In other words, the pumped region of a crystal with WGM-type modes gradually becomes more and more transparent to exciting radiation. This explains the saturation of the $I_{int}(\rho_{exc})$ dependence at $\rho_{exc} > 50 - 60$ kW/cm^2.

In the regions of the film A with large close-packed microcrystallites, the excitation of WGM-type modes is difficult as a result of optical losses due to close contact between crystallites. In this regard, only FPMs provide the necessary gain for ASE, which manifests itself as a single superlinear segment in the $I_{int}(\rho_{exc})$ dependence. The absence of ASE at RT in the case of the film B is explained by large losses in relatively small close-packed microcrystallites.

In contrast to the RT case, at low temperature there are no saturation in the $I_{int}(\rho_{exc})$ dependence and, in general, a two-threshold character of radiation for the excitation range used. This suggests the absence of transition to another type of radiation, which is ensured by the higher radiative activity of recombining excitons at low temperature compared to RT, as well as greater stability of excitons, lower reabsorption of exciton radiation, and thermally less occupied upper energy states, which is necessary for *X*-*X* scattering process. As a result, at a low temperature *P* band can be excited in a wide range of excitation intensities and has a lower threshold compared to stimulated emission resulting from the *X*-*m*LO processes, as well as emission in the EHP [34].

Conclusions

We have demonstrated the possibility of synthesizing ZnO film structures with laser properties by pyrolytic carbothermal synthesis. The radiative properties of such films are affected by both the size of microcrystallites and their packing density. In particular, it was found that the loose-packed structure of large microcrystallites provides a greater amplification of spontaneous emission in the near UV region compared to close-packed structure at room temperature. An analysis of the temperature behavior of the films' NBE emission, taking into account the previously obtained data, allowed us to establish the cause of the observed phenomenon. It was associated with the action of exciton-electron scattering in addition to the main mechanism, which is two-phonon assisted exciton radiation. Saturation of this additional mechanism as a result of weak localization of subsurface optical modes of the WGM type causes the appearance of a second range of superlinear growth in the dependence of the radiation intensity vs. pumping power. Thus, the formation of the loose-packed structure of microcrystallites in a ZnO film may result in an additional intensification of UV ASE due to providing an additional gain mechanism.

The results obtained open up more widely the possibilities of the thermal evaporation synthesis. They can be useful in optimizing the properties of ZnO laser micro- and nanostructures and interpreting the mechanisms of spontaneous and stimulated emissions in them. Laser ZnO film structures can be useful for production of high-power UV light emitting diodes, as well as for pumping in visible light sources.

References

[1] Capper P, Kasap SO, Willoughby A. Zinc oxide materials for electronic and optoelectronic device applications. New York: John Wiley and Sons; 2011. DOI: 10.1002/9781119991038.

[2] Rong P, Ren S, Yu Q. Fabrications and applications of ZnO nanomaterials in flexible functional devices-a review. Crit Rev Analyt Chem 2019; 49: 336-349. DOI: 10.1080/10408347.2018.1531691.

[3] Borysiewicz MA. ZnO as a functional material, a review. Crystals 2019; 9: 505. DOI: 10.3390/cryst9100505.

[4] Murzin SP, Kazanskiy NL. Arrays formation of zinc oxide nano-objects with varying morphology for sensor applications. Sensors 2020; 20: 5575. DOI: 10.3390/s20195575.

[5] Murzin SP. Improvement of thermochemical processes of laser-matter interaction and optical systems for wavefront shaping. Appl Sci 2022; 12: 12133. DOI: 10.3390/app122312133.

[6] Murzin SP, Kazanskiy NL, Osipov S. Formation of zinc oxide nanoobjects arrays for electrically switchable diffraction gratings. Proc SPIE 2022; 12295: 122950F. DOI: 10.1117/12.2631728.

[7] Özgür Ü, Hofstetter D, Morkoc H. ZnO devices and applications: a review of current status and future prospects. Proc IEEE 2010; 98(7): 1255-1268. DOI: 10.1109/JPROC.2010.2044550.

[8] Versteegh MA, Vanmaekelbergh D, Dijkhuis JI. Room-temperature laser emission of ZnO nanowires explained by many-body theory. Phys Rev Lett 2012; 108: 157402. DOI: 10.1103/PhysRevLett.108.157402.

[9] Xu C, Dai J, Zhu G, Zhu G, Lin Y, Li J, Shi Z. Whispering-gallery mode lasing in ZnO microcavities. Laser Photonics Rev 2014; 8: 469-494. DOI: 10.1002/lpor.201300127.

[10] Klingshirn CF. Semiconductor optics. 4th ed. Berlin: Springer; 2012. ISBN: 9783642283628.

[11] Galdámez-Martinez A, Santana G, Güell F, Martínez-Alanis PR, Dutt A. Photoluminescence of ZnO nanowires: a review. Nanomaterials 2020; 10: 857. DOI: 10.3390/nano10050857.

[12] Aspoukeh PK, Barzinjy AA, Hamad SM. Synthesis, properties and uses of ZnO nanorods: a mini review. Int Nano Lett 2022; 12: 153-168. DOI: 10.1007/s40089-021-00349-7.

[13] Li LE, Demianets LN. Room-temperature excitonic lasing in ZnO tetrapod-like crystallites. Opt Mater 2008; 30: 1074-1078. DOI: 10.1016/j.optmat.2007.05.013.

[14] Demyanets LN, Li LE, Lavrikov AS, Nikitin SV. Nanocrystalline zinc oxide: pyrolytic synthesis and spectroscopic characteristics. Crystallogr Rep 2010; 55: 142-148. DOI: 10.1134/S1063774510010219.

[15] Tarasov AP, Muslimov AE, Kanevsky VM. Excitonic mechanisms of stimulated emission in low-threshold ZnO microrod lasers with whispering gallery modes. Materials 2022; 15: 8723. DOI: 10.3390/ma15248723.

[16] Tarasov AP, Briskina CM, Markushev VM, Zadorozhnaya LA, Lavrikov AS, Kanevsky VM. Analysis of laser action in ZnO tetrapods obtained by carbothermal synthesis. JETP Lett 2019; 110: 739-743. DOI: 10.1134/S0021364019230115.

[17] Galli G, Coker JE. Epitaxial ZnO on sapphire. Appl Phys Lett 1970; 16: 439-441. DOI: 10.1063/1.1653058.

[18] Nickel NH, Terukov E. Zinc oxide – a material for micro- and optoelectronic applications. Springer Science & Business Media; 2005.

[19] Zadorozhnaya LA, Tarasov AP, Volchkov IS, Muslimov AE, Kanevsky VM. Morphology and luminescence of flexible free-standing ZnO/Zn composite films grown by vapor transport synthesis. Materials 2022; 15: 8165. DOI: 10.3390/ma15228165.

[20] Zhang Z, Yates JT Jr. Band bending in semiconductors: chemical and physical consequences at surfaces and interfaces. Chem Rev 2012; 112: 5520-5551. DOI: 10.1021/cr3000626.

[21] Wang L, Giles NC. Temperature dependence of the free-exciton transition energy in zinc oxide by photoluminescence excitation spectroscopy. J Appl Phys 2003; 94: 973-978. DOI: 10.1063/1.1586977.

[22] Klingshirn C, Fallert J, Zhou H, Sartor J, Thiele C, Maier-Flaig F, Schneider D, Kalt H. 65 years of ZnO research – old and very recent results. Phys Status Solidi 2010; 247: 1424-1447. DOI: 10.1002/pssb.200983195.

[23] Foreman JV, Simmons JG, Baughman WE, Liu J, Everitt JO. Localized excitons mediate defect emission in ZnO powders. J Appl Phys 2013; 113: 133513. DOI: 10.1063/1.4798359.

[24] Tarasov AP, Venevtsev ID, Muslimov AE, Zadorozhnaya LA, Rodnyi PA, Kanevsky VM. Luminescent properties of a ZnO whisker array as a scintillation detector material. Quantum Electron 2021; 51: 366-370. DOI: 10.1070/QEL17534.

[25] Ozgur U, Alivov YI, Liu C, Teke A, Reshchikov MA, Dogan S, Avrutin V, Cho SJ, Morkoc H. A comprehensive review of ZnO materials and devices. J Appl Phys 2005; 98: 41301. DOI: 10.1063/1.1992666.

[26] Zimmler MA, Capasso F, Müller S, Ronning C. Optically pumped nanowire lasers: invited review. Semicond Sci Tech 2010; 25: 024001. DOI: 10.1088/0268-1242/25/2/024001.
[27] Klingshirn C. The luminescence of ZnO under high one- and two-quantum excitation. Phys Status Solidi B 1975; 71: 547-556. DOI: 10.1002/pssb.2220710216.
[28] Matsuzaki R, Soma H, Fukuoka K, Kodama K, Asahara A, Suemoto T, Adachi Y, Uchino T. Purely excitonic lasing in ZnO microcrystals: Temperature-induced transition between exciton-exciton and exciton-electron scattering. Phys Rev B 2017; 96: 125306. DOI: 10.1103/PhysRevB.96.125306.
[29] Tempel JS, Veit F, Aßmann M, Kreilkamp LE, Rahimi-Iman A, Löffler A, Höfling S, Reitzenstein S, Worschech L, Forchel A, Bayer M. Characterization of two-threshold behavior of the emission from a GaAs microcavity. Phys Rev B 2012; 85: 075318. DOI: 10.1103/PhysRevB.85.075318.
[30] Niyuki R, Fujiwara H, Nakamura T, Ishikawa Y, Koshizaki N, Tsuji T, Sasaki K. Double threshold behavior in a resonance-controlled ZnO random laser. Apl Photonics 2017; 2: 036101. DOI: 10.1063/1.4974334.
[31] Moss TS. Theory of intensity dependence of refractive index. Phys Status Solidi 1980; 101: 555-561. DOI: 10.1002/pssb.2221010214.
[32] Kamat PV, Dimitrijevic NM, Nozik AJ. Dynamic Burstein-Moss shift in semiconductor colloids. J Phys Chem 1989; 93: 2873-2875. DOI: 10.1021/j100345a003.
[33] Klingshirn C, Hauschild R, Fallert J, Kalt H. Room-temperature stimulated emission of ZnO: Alternatives to excitonic lasing. Phys Rev B 2007; 75: 115203. DOI: 10.1103/PhysRevB.75.115203.
[34] Koch SW, Haug H, Schmieder G, Bohnert W, Klingshirn C. Stimulated intrinsic recombination processes in II–VI compounds. Phys Status Solidi 1978; 89: 431-440. DOI: 10.1002/pssb.2220890212.

Authors' information

Ludmila Alexandrovna Zadorozhnaya (b. 1944), PhD, graduated from Lomonosov Moscow State University in 1968, majoring in Geochemistry. Currently she is a lead researcher at the Laboratory for Growth of Thin Films and Inorganic Nanostructures of A.V. Shubnikov Institute of Crystallography, FSRC "Crystallography and Photonics" of RAS. Her research focuses on growth methods of semiconductor nano/microstructures and organic crystals.
E-mail: *cvdlab@crys.ras.ru*

Andrey Petrovich Tarasov (b. 1990), PhD, graduated from National Research Nuclear University "MEPhI" in 2013, majoring in Solid State Physics, Nanostructures and Superconductivity. He is a researcher at the Laboratory for Growth of Thin Films and Inorganic Nanostructures of A.V. Shubnikov Institute of Crystallography, FSRC "Crystallography and Photonics" of RAS. His research focuses on solid state photonics, particularly, luminescence and lasing of semiconductor nano- and microstructures and films. He also works at Vladimirsky Research and Clinical Institute "MONIKI", where his research interests include non-invasive optical techniques of medical diagnostics and some aspects of the radiative transfer theory. E-mail: *tarasov.a@crys.ras.ru*

Alexander Sergeevich Lavrikov (b.1953), PhD, graduated from Moscow Engineering and Physics "MEPhI" in 1977, majoring in Metallurgical Science. He is a lead engineer at the Laboratory for Growth of Thin Films and Inorganic Nanostructures of A.V. Shubnikov Institute of Crystallography, FSRC "Crystallography and Photonics" of RAS. His work focuses on growth methods of semiconductor films and nano/micro structures. E-mail: *a.lawrikow@mail.ru*

Vladimir Mikhailovich Kanevsky (b. 1948), PhD, Dr. Sci., graduated from Moscow Institute of Steel and Allows in 1971, majoring in Semiconductor Physics. Currently he works as a head of the Laboratory for Growth of Thin Films and Inorganic Nanostructures of A.V. Shubnikov Institute of Crystallography, FSRC "Crystallography and Photonics" of RAS. His research interests are solid state physics, growth and physical properties of semiconductor crystals, surface science. E-mail: *kanev@crys.ras.ru*

Received August 24, 2023. The final version – January 26, 2024.